NIKHEF - NATIONAL INSTITUTE FOR SUBATOMIC PHYSICS-

Energy calibration procedure of a pixel detector

R. P. M. van der Boog
The Hague university of applied sciences
Bachelor thesis of applied physics (B. Eng)

June 2013

Energy calibration procedure of a pixel detector

HBO graduation internship

Author: Rob van der Boog
Student number: 09061630
Technische natuurkunde

Supervisors Nikhef

E. Jr. Schioppa M.Sc.
Dr. Ing. N. van Bakel

Supervisors The Hague University

Ing. C.A. Swarts
Dr. L. H. Arntzen

Commissioner

Ing. K. Hoogendijk

February – June 2013

Abstract

In the medical community, X-rays are an important tool in imaging the human body. In principle X-ray images are 2 dimensional images. By measuring such X-ray images at multiple angles, one can construct the 3 dimensional inner structure of the sample. This 3 dimensional structure is created by applying a computerized tomography algorithm (CT-reconstruction) on the multiple angle X-ray images. Currently, artifacts appear in the 3 dimensional structure because little or no spectral information is used in the CT-reconstruction. At Nikhef, research is carried out to study the possibility to improve CT-reconstruction by exploiting the spectroscopic capabilities of pixel detectors from the Medipix family.

In this thesis, an energy calibration is performed for one of these detectors, a Timepix detector. The calibration is performed using X-ray fluorescence emitted by several pure materials. A Timepix detector consists of four pixel devices, each consisting of 256 by 256 pixels. During this project, the Timepix detector is calibrated on a global (per device) and per pixel scale, using C++ analysis software.

The first version of the per-pixel analysis software had an efficiency of less than 75%, because the ranges were initialized on a global scale. The global range also caused several pixels to repeatedly fall out of range, leading to pixels without a calibration. Therefore the algorithm is enhanced during this project, leading to a new efficiency of at least 90%. Next to this the new algorithm is completely independent from any global parameters, leading to almost 100% of the pixels to be calibrated correctly.

Contents

1 Introduction 1
1.1 Beam hardening 1
1.2 Aim of the project 1
2 X-ray photons 3
2.1 X-ray research analysis tube 3
2.2 Bremsstrahlung 3
2.3 Characteristic spectrum of X-ray tube 4
2.4 Fluorescence 6
3 Pixel detectors 8
3.1 Sensor 8
3.1.1 Charge sharing 9
3.2 Timepix 9
3.2.1 Analog circuitry 10
3.2.2 Digital circuitry 10
3.3 Software 10
3.3.1 Equalization 10
3.3.2 Threshold scan 11
4 Calibration 12
4.1 Source 12
4.2 Fitting function 13
Global analysis 14
4.3 Per pixel analysis 15
4.3.1 First estimation 16
4.3.2 Per pixel fit 17
4.4 Calibration 18
5 Discussion 20

6 References 21
6.1 Publications 21
6.2 Books 21
6.3 Web sources 21

List of symbols:

E	energy	[eV]
$N_{e\text{-}h}$	number of electron-hole pairs	
Q	charge	[C]
e	charge of an electron	[$-1.6022 \cdot 10^{-19}$ C]
N	number of photon counts	
$f(x)$	Gaussian distribution	
$erf(x)$	error function	
$G(THL)$	Gaussian distribution of counted photons	
$C(THL)$	charge sharing	
$B(THL)$	constant background	
$S(THL)$	measured spectrum	
$F(THL)$	fit function	
μ	position of Gaussian	
σ	width of Gaussian	
NE	charge sharing slope	
$scale$	function scale	
$scale_{\beta/\alpha}$	relative amount between Kα and Kβ	
$offset$	function offset	

1 Introduction

Within the medical community, X-rays are an important tool for imaging the inner part of a human body. The principle of X-ray imaging is relatively simple: when a known amount of X-ray photons are transmitted through an object, the amount of photons detected behind the object is reduced by absorbance of the object. Such transmission values thus contain information about object inner structure. Conventional X-ray images consist of intensity maps of X-ray photons. By collecting X-ray images (called projections) at different angles of view, it is possible to estimate the 3D inner structure of the object using a reconstruction algorithm. Such a technique is called X-ray computerized tomography (CT).

Photon detection is the crucial part of X-ray imaging. R&D on the detector side is required in order to improve the imaging capabilities of X-ray systems. At Nikhef - National institute for Subatomic physics -, a research project is carried out to study the possibility to improve X-ray imaging with pixel detectors from the Medipix family. These pixel detectors are described in chapter 3.

1.1 Beam hardening

Although X-ray tubes emit a polychromatic spectrum, conventional X-ray detectors do not have an energy discriminating capability. High energy photons have a lower probability to be absorbed while traveling through an object than low energy photons. Thus the average energy of the transmitted spectrum increases while passing through an object. This phenomenon is called beam hardening. Beam hardening causes artifacts in CT because little or no spectral information is taken into account in the reconstruction. It is particularly enhanced when the object is composed of two or more materials with a big difference in absorption coefficient. Figure 1 shows a CT reconstruction of a human jaw, where two high Z material implanted teeth show evident beam hardening artifacts. Beam hardening artifacts is an unwanted phenomenon because it might be confused with features of the body, in which case a wrong diagnoses can be established.

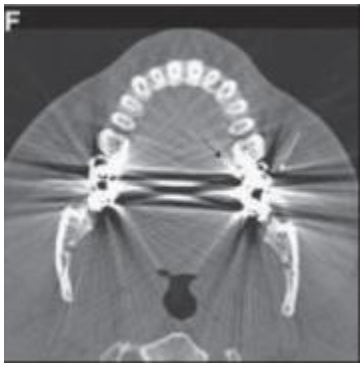

Figure 1: CT scan of a jaw. Beam hardening occurs in correspondence of the metal implantations in the molars on both sides [7].

1.2 Aim of the project

The recent development and availability of spectroscopic X-ray detectors opens up the possibility to develop techniques that, taking into account the spectral information alongside conventional intensity mapping, would get rid of, or at least reduce the effect of beam hardening in CT. Understanding the properties of these detectors, in particular their energy response, is of primary importance.

In this project an energy calibration technique has been developed for one of these detectors, the Timepix detector. This technique provides a powerful tool to determine the energy response of each of the pixels composing the detector, individually.

This thesis is a bachelor graduation project regarding energy calibration for a detector from the Medipix family. Medipix detectors provide the opportunity to measure photon energy. Construction of a energy calibration is explained after some general information about detectors and X-rays.

2 X-ray photons

X-rays were discovered by Wilhelm Conrad Röntgen during discharge tube experiments. Röntgen observed the emission of an unknown radiation and therefore called it X-rays [4]. Later on it was demonstrated that X-rays are high energy photons. Such photons have a wavelength of 0.01 nm to 1 nm, corresponding to energies of 100 keV and 1 keV, respectively. X-rays are mainly used in imaging and material determination.

2.1 X-ray tube

The X-ray source installed in the Nikhef setup is a Hamamatsu microfocus (focal size 5 µm at 4 W) X-rays source type L9421-02. It operates at a tube potential between 20 – 90 kV and a maximum tube current of 200 µA (current is voltage dependant, appendix E). Additional information about the Hamamatsu device can be found in this appendix.

The Hamamatsu device is an X-ray tube. Figure 2 shows a simplified view of X-ray creation inside the X-ray vacuum tube.

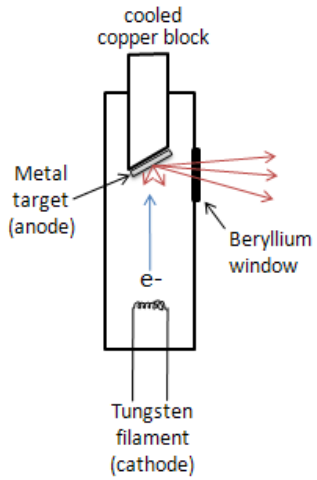

Figure 2: Principle of X-ray tubes [10].

Main components in Figure 2 are the anode and cathode in a vacuum tube. The cathode is constituted of a thin filament which emits free electrons by thermionic effect. Under the influence of an electric potential between anode and cathode the free electrons start to accelerate towards the anode. The maximum electron energy is determined by the electric potential between cathode and anode. Most electrons that reach the anode convert their energy into heat. However, some electrons emit photons by bremsstrahlung or will induce the emission of characteristic X-rays. These two cases are described in the following paragraphs.

2.2 Bremsstrahlung

Some electrons pass in close proximity of the nuclei of the atoms composing the anode material. Due to the large electric field of these nuclei, the passing electrons trajectory is bend. This causes the electron to release part of its energy in the emission of a photon [5], see Figure 3. This phenomenon is called bremsstrahlung, a German term for “braking radiation”.

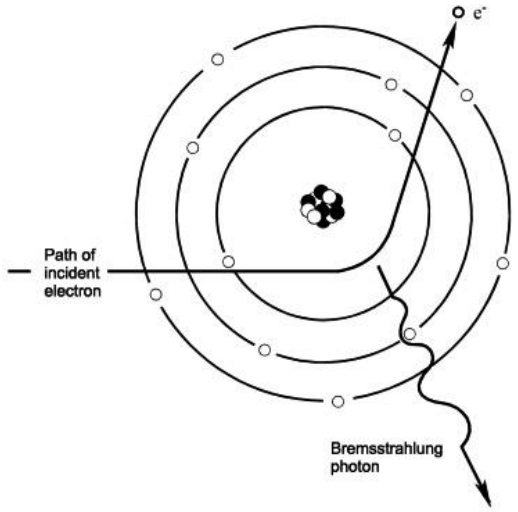

Figure 3: Model of bremsstrahlung emission [11].

The amount of energy lost depends on the distance between the electron and nucleus [5]. Closer impact parameters give an increased electric field seen by the electron, thus providing more acceleration. In other words, electrons passing in closer proximity lose more kinetic energy and thus emit higher energy X-rays. Next to this, electrons have a higher probability to pass the nucleus from a larger distance. This causes an increased intensity for lower photon energies.

Due to the combination of effects, Bremsstrahlung shows a continuous spectrum which is independent of the used anode material [5], see Figure 4.

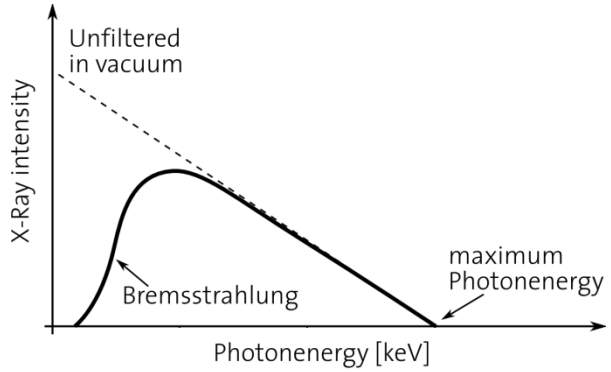

Figure 4: Continuous spectrum due to bremsstrahlung from an X-ray tube.
The dashed line shows the spectrum in vacuum[12].

Figure 4 is also a good example to see the effect of beam hardening. The spectrum generated by the X-ray tube has a typical shape as shown by the dashed line. However, due to the absorption from the vacuum tube beryllium window, a decrease of intensity occurs at lower energy, shifting the average energy of the spectrum towards a higher value (hardening of the beam). The resulting spectrum outside the tube is shown by the thicker line.

2.3 Characteristic spectrum of X-ray tube

Some incident electrons collide with the electrons that are bound to the nucleus. When the energy of the incident electrons exceeds the binding energy of the orbiting electron, this latter is released from the atom, leaving a vacancy in the shell [5]. Such vacancy is filled by an electron belonging to a higher energy

level. During the transition to the vacancy the energy difference is emitted, in most of the cases as a photon. Photon energy will be equal to equation 2.1:

$$E_\lambda = E_1 - E_2 \tag{2.1}$$

with:

E_λ	photon energy	[keV]
E_1	discrete energy of the transition electron	[keV]
E_2	discrete energy of the vacancy shell	[keV]

Electron levels have discrete energy values, which are characteristic of the element. If electron levels are discrete, so are the electronic transitions between these electron levels. Therefore the emitted radiation from electronic transition in the atom is monochromatic. Figure 5 shows the first four electron shells, K,L,M and N.

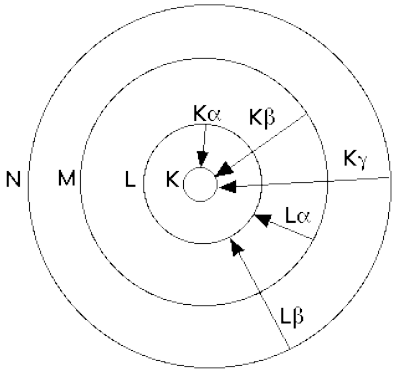

Figure 5: Electron shells and the naming of characteristic photons [13]

For materials with an higher atomic number than Sodium (Na), electron transitions to the K shell emits a photon with energies in the X-ray range. The name given to the photon is determined by the origin of the electron transition and the vacancy shell. Figure 5 shows both the alphabetic and Greek characters used in naming the photon. The alphabetic ones are the shells containing the vacancy, with quantum number 1 being the K shell. Whereas the Greek characters show the origin of the electron, with α being the first shell after the vacancy shell and β,γ being the second and third respectively [5]. Notice that a Kβ transition has a higher energy difference than a Kα transition, and therefore gives rise to a higher energy X-ray. For example, if a vacancy in the K-shell of tungsten is filled with an electron from the L-shell, a Kα photon is emitted. This photon would have an energy equal to [5]:

$$E_\lambda = (-10.2\ \text{keV}) - (-69.5\ \text{keV}) = 59.3\ \text{keV}$$

Within the actual X-ray tube spectrum both bremsstrahlung and characteristic X-rays are superimposed, as can be seen in Figure 6. Characteristic radiation is typical of the anode material.

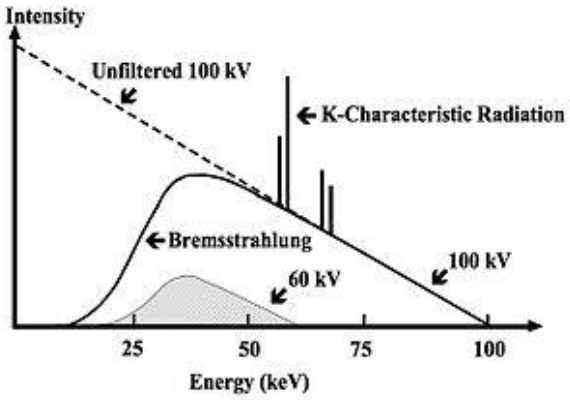

Figure 6: Superimposed bremsstrahlung and characteristic spectrum from an X-ray tube with tungsten anode, operated at 100 kV. Also shown in grey is a 60 kV spectrum, showing a lower X-ray intensity. [14]

2.4 Fluorescence

X-ray fluorescence is the emission of a photon caused by electron transition in the electronic structure of an atom. In case of fluorescence the vacancy required for electron transition is induced by a photon. The electron transition itself occurs similar to the characteristic X-ray phenomenon, emitting photons characteristic of the target material.

During this project a detector is calibrated with monochromatic fluorescence light emitted from different targets. These fluorescence photons are emitted isotropically (in every direction). In order to avoid the primary beam to be detected, the detector is positioned as shown in Figure 7.

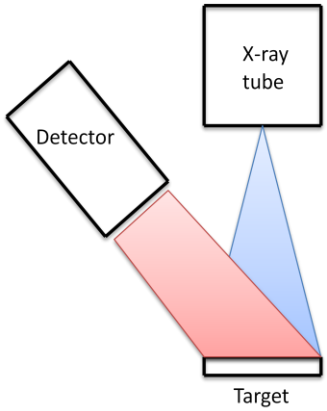

Figure 7: Fluorescence setup. Positioning the detector in the backside ensures direct photons from the X-ray tube to be disregarded.

With this setup, Kα and Kβ emission from a series of targets are measured. Used targets are displayed in Table 1, showing a list of the pure materials with corresponding emitted energies.

Table 1: Fluorescence targets with corresponding energies, abbreviations and atom numbers (Z)

Atom number	Materials	Abbreviation	Kα (KeV)	Kβ (keV)
28	Nickel	Ni	7.477	8.264
29	Copper	Cu	8.047	8.904
30	Zinc	Zn	8.638	9.571
40	Zirconium	Zr	15.774	17.666
46	Palladium	Pd	21.175	23.816
47	Silver	Ag	22.162	24.942
49	Indium	In	24.207	27.274
50	Tin	Sn	25.270	28.483

3 Pixel detectors

Pixel devices are known for their use in photo camera's. Next to this they are also used in high energy physics and radiation experiments, such as X-ray imaging. One family of pixel devices is the Medipix family. This series of devices emerged from a collaboration[1] project with numerous European universities and Research Institutes, hosted by CERN. Currently there are four pixel devices in the Medipix family; Medipix1, Medipix2, Medipix3 and Timepix. The latter is a device derived from the design of Medipix2, with some functions that differ from the Medipix ones. Detectors in the Medipix family are single photon counting detectors, which means they detect single photons and count the total amount of photons during a measurement.

Medipix are pixellated readout chips. In order to make a full detector, they must be connected to a radiation sensitive medium. For X-ray imaging, this detection medium is usually a 300 μm thick Silicon sheet which is bump bonded to the chip. A simplified view of the combined components can be seen in Figure 8.

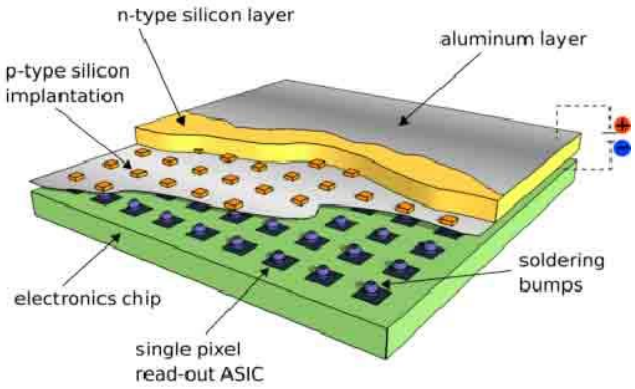

Figure 8: Simplified view of a sensor bump bonded to a readout chip [8].

3.1 Sensor

Single incident high energy photons such as X-rays are able to release photoelectrons in the sensor. Photoelectrons are electrons which are freed by photoelectric effect. The photoelectron has the same energy of the original photon. Once the electron is freed, it travels through the sensor material and produces secondary electrons along its track, emitted by ionization. Ionization is the separation of a bounded electron from its atom due to the energy release of a particle, in this case the photoelectron. When ionization occurs in a semiconductor, the electron leaves a vacancy (called hole) which behaves like a positive charge carrier. The minimum energy required to free an electron-hole pair is equal to the ionization energy. In silicon this corresponds to the energy gap between the valence band and the conduction band, E_{gap} = 1.12 eV. The average energy required to create an electron-hole pair in silicon is, instead $E_{e\text{-}h}$ = 3.6 eV. Therefore, a photoelectron of a given energy produces, on average, a well defined number of electron-hole pairs, given by [6]:

$$N_{e-h} = \frac{E_{ph}}{E_{e-h}} \tag{3.2}$$

[1] Collaboration partners are listed on this site: http://medipix.web.cern.ch/medipix/pages/medipix2/documentation.phphttp://medipix.web.cern.ch/medipix/pages/medipix2/collaboration.php

with :

$N_{e\text{-}h}$	number of electron hole pairs	[-]
E_{ph}	energy of the photoelectron	[keV]
$E_{e\text{-}h}$	average energy to create an e-h pair	[keV]

In order to collect the charge carriers and thus create a detectable signal, a bias voltage of 100 V is applied between the electrodes of the sensor.. Under influence of this bias voltage electrons and holes travel towards different electrodes. Depending on the applications, detectors can be made to collect either electrons or holes. The detector used in this project is set to collect holes, i.e. the pixels have a positive polarity. The total charge collected is equal to the amount of e-h pairs created times the charge of a hole. This leads to equation 3.3 [6]:

$$Q_{total} = \frac{E_{ph}}{E_{e-h}} \cdot (-e) \tag{3.3}$$

with:

Q_{total}	average total charge	[C]
e	charge of an electron	[-1,6022·10^{-19} C]

3.1.1 Charge sharing

Due to thermal diffusion the motion of electrons and holes also has a component transversal to the drift field. Therefore the cloud of charge carriers created by the photon conversion tends to spread out while drifting towards the collection electrode. In finely segmented detectors, especially pixel detectors, this causes a phenomenon called charge sharing. When a photon is converted in the boundary region between two or more pixels, the charge cloud is shared between these pixels. Shared charge is less than the total charge, and will therefore be interpreted as a lower energy photon. As a consequence, multiple lower energy photons can be detected from a single incident photon. This phenomenon is particularly detrimental for X-ray detectors with spectral capabilities.

3.2 Timepix

Timepix chips consist of a 256 x 256 matrix with 55 µm x 55 µm pixels[2]. The total chip dimensions are 16 mm x 14 mm. Timepix chips are three side buttable with on the fourth side a non-sensitive area of 2 mm x 14 mm used to connect the peripherical circuitry [1]. The non-sensitive area is where the chip bias is applied and data is transferred. Each individual pixel has a circuitry which can be separated into an analog and digital part [1], see Figure 9.

[2] During this project a quad detectors is used. Quad detectors have four chips in a 2x2 matrix with a single silicon sensor overlaying all chips.

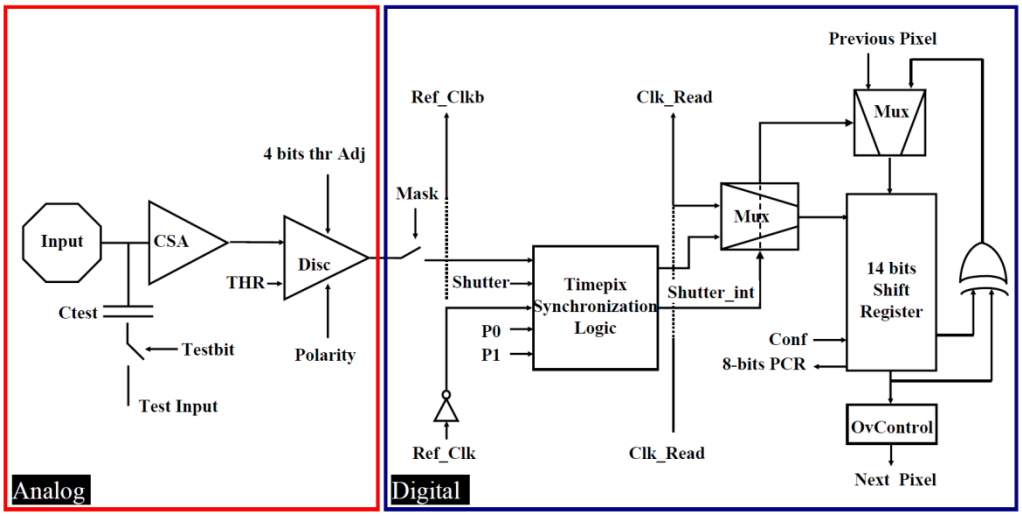

Figure 9: Analog and digital circuitry of a single pixel from a Timepix device. [1]

3.2.1 Analog circuitry

Once holes reach the collection electrode of the pixel, they enter the analog side of the circuitry. This side consists of a pre-amplifier and a discriminator, as shown in Figure 9. The pre-amplifier implemented in Timepix is charge sensitive (CSA), producing a voltage step output which is proportional to the collected charge [2]. From here the signal is sent to the discriminator. The discriminator compares the signal with a fixed threshold value (THL). Signals which exceed THL are send to the digital side for further processing, while the others are disregarded. In this way a pixel is set to measure all photons whose energy exceeds the energy determined by THL.

3.2.2 Digital circuitry

Figure 9 also shows the digital part of the circuitry. The main component in this part is the Timepix Synchronization Logic (TSL) and the shift register [1]. The TSL controls the discriminator in the analog part. It also sends a signal to the shift register if the discriminator conditions are met. The shift register stores all the signals until the end of the measurement. In other words, when THL is exceeded, TSL emits a signal, and the shift register stores one photon count. The shift register has a maximum count capacity, which is 11810 [1]. The consequence is that a single measurement cannot store more than 11810 photons per measurement. In order to acquire more data, multiple measurements have to be performed consecutively. The dead time between successive measurements depends on the readout hardware and software. In most of the cases, the user can operate the device with a negligible dead time.

3.3 Software

The software package used to read the output of the chip is called Pixelman[3]. Pixelman is a program made by the Medipix group of the Czech Technical University (CTU) in Prague [9]. The software is specially made to operate Medipix2 and Timepix based devices. The GUI allow to visualize the acquired frames and to write data in text files.

3.3.1 Equalization

Pixels in Medipix devices are designed to be identical to one another. However, due to natural mismatches that occur during the processing, some parameters may vary from pixel to pixel. In particular, the global value of threshold may translate to a local value which is different from pixel to pixel.

[3] Additional information about Pixelman is available at:
http://aladdin.utef.cvut.cz/ofat/others/Pixelman/Pixelman.html

Pixelman provides a function to equalize for variations in threshold using a method called noise floor equalization [2]. In order to correct for threshold inequalities, the Timepix device exploits four bits dedicated to threshold adjustment for every pixel. This system allows to fine tune the THL offset with 16 adjustment steps for every pixel. The steps are applied on the discriminator using the "4 bit thl Adj" input, shown in the analog part of Figure 9. The size of the adjustment steps is determined by the THS DAC parameter [2], which can also be optimized before scanning.

The noise floor equalization starts at adjustment step zero, gradually moving the THL (into the noise) until each pixel has reached a criteria in photon counts. Corresponding pixels are shown in the equalization graph at the THL value where the criterion was met. Doing so for every pixel will eventually lead to the distribution of the pixel THL positions, as can be seen from the blue Gaussian in Figure 10. Performing the same measurement for the second adjustment step would lead to a similar Gaussian, shifted to another THL value. Doing so for every adjustment step, a linear trend would appear for the THL offset. Therefore, a measurement with the first and last step is enough to extrapolate the THL values for all the intermediate adjustment steps [2]. The adjustment step for each pixel is chosen in such a way, that the distribution of pixels is minimized. This is shown in the black distribution in Figure 10.

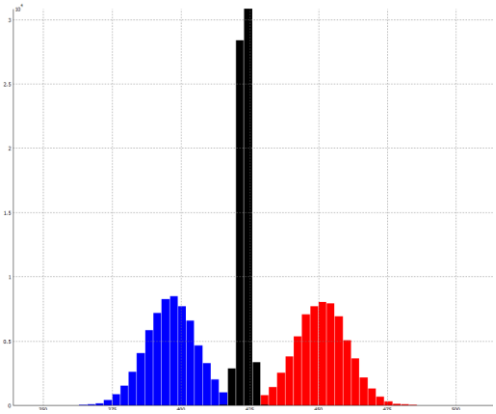

Figure 10: A single chip equalization histogram, with on the horizontal axis THL values, and a vertical axis showing the number of pixels. The blue dispersion corresponds to adjustment step zero, whereas the red corresponds to adjustment step 15. The dispersion in black shows the final distribution after equalization.

3.3.2 Threshold scan

During this project, all measurements are performed in the threshold scan window of Pixelman. A threshold scan is a collection of multiple measurements at different THL values. In this way the integral of the measured spectrum is obtained. The threshold scan has several parameters which are possible to set:

- Minimum and maximum of THL range
- Step size (change in THL after each measurement)
- Time of each measurement
- Frames (number of acquisitions per step)

4 Calibration

The cumulative spectrum is measured using the threshold scan (THL scan) of Pixelman. This is repeated for each target. The spectra are known to contain information about Kα and Kβ. In this chapter is discussed how the THL values of Kα and Kβ are determined, after giving some information about the spectrum.

4.1 Source

In principle the spectrum emitted by a fluorescence target contains two monochromatic peaks, Kα and Kβ. In order to explain the spectrum a single monochromatic peak is considered, as can be seen in Figure 11.

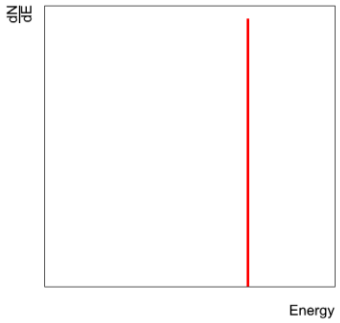

Figure 11: Monochromatic radiation.

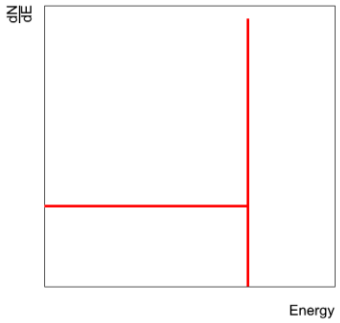

Figure 12: Monochromatic radiation plus charge sharing.

A fraction of the monoenergetic photons will undergo charge sharing. The effect of charge sharing on the detected spectrum is a partial deployment of the monochromatic peak into a tail at lower energies. At first approximation the probability to detect any energy below the incident energy is constant, thus giving a constant tail in the spectrum, as shown in Figure 12.

Monochromatic radiation emitted by the target is absorbed in the sensor. The signal created follows on average equation 3.3, with fluctuations due to the stochastic nature of the interaction of the photoelectron with matter. This phenomenon characterizes the energy resolution of the detector. Its effect on monochromatic radiation and charge sharing can be seen in Figure 13.

As explained in paragraph 3.2.1, all photons with an energy exceeding THL are measured. By measuring THL in steps from high energy to low energy, the amount of photons measured increases at each THL step. Resulting in the integral of the measured spectrum, shown in Figure 14.

THL values are expressed in arbitrary units provided by the chip readout. Due to the sensor polarity (hole collecting) high energy threshold correspond to low THL values, and low energy threshold to high energy values. Resulting in a inverted x-axis if THL is evaluated.

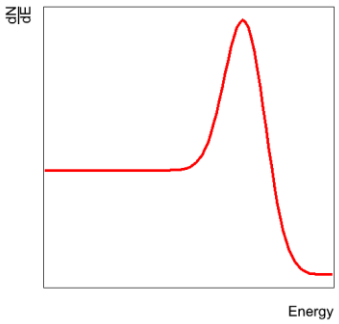

Figure 13: Measured spectrum

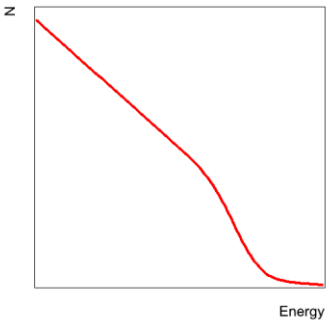

Figure 14: Integral of the measured spectrum.

One way to determine the THL values of Kα and Kβ is by differentiating the cumulative spectrum and fitting the photopeak. However doing so yields a noisy spectrum, where the visibility of photopeaks is low. For this reason, in this project the cumulative spectrum is fitted directly, and the parameters are used to retrieve the spectrum.

4.2 Fitting function

The function describing the cumulative spectrum from a monochromatic radiation source has three components, the Gaussian photopeak, charge sharing and background. Mathematically, a Gaussian is writtend as:

$$f(x) = e^{-x^2} \tag{4.4}$$

This Gaussian has a bell shape, shown in Figure 24 appendix A. Applied on the measurement, it has a certain position and width (Figure 25):

$$G(THL) = \frac{1}{\sigma\sqrt{2\pi}} e^{-\frac{(THL-\mu)^2}{2\sigma^2}} \tag{4.5}$$

with:

μ	position of Gaussian
σ	width of Gaussian

Function 4.5 is normalized to 1. A charge sharing component pairs to each photopeak. Due to the Gaussian nature of the fluctuations in energy, the charge sharing tail of figure 12 is smeared out by the energy resolution according to an error function. The error function is defined as:

$$erf(x) = \frac{2}{\sqrt{\pi}} \int_0^x e^{-t^2} dt \tag{4.6}$$

An example of an error function is shown in Figure 26, appendix A. Applied on a measurement, the error function has the form:

$$C(THL) = \frac{NE}{2}\left(1 + erf\left(\frac{THL - \mu}{\sqrt{2}\cdot\sigma}\right)\right) \tag{4.7}$$

with:

NE charge sharing fraction with respect to the photpeak

Notice that μ and σ in 4.7 are the same as in 4.5.

The final component is the background. Background is approximated as a constant value. Adding all three components yields the spectrum defined by equation 4.8 and shown in Figure 28:

$$S_\alpha(THL) = scale\cdot\left[G_\alpha(THL) + C_\alpha(THL)\right] + B(THL) \tag{4.8}$$

with:

scale scale factor accounting for photon statistics

The cumulative spectrum is obtained by integrating equation 4.8:

$$F_\alpha(THL) = scale\cdot\int_{-\infty}^{THL}\left[G_\alpha(THL) + C_\alpha(THL)\right]\cdot dTHL + \int_{-\infty}^{THL} B(THL)\cdot dTHL \tag{4.9}$$

The measured spectrum contains monochromatic radiation from both Kα and Kβ. Therefore, in the most general form of 4.9, a second Gaussian and charge sharing components are introduced, containing parameters of Kβ:

$$\begin{aligned} F_{\alpha,\beta}(THL) = {} & scale\cdot\int_{-\infty}^{THL}\left[G_\alpha(THL) + C_\alpha(THL)\right]dTHL + \\ & scale_\beta\int_{-\infty}^{THL}\left[G_\beta(THL) + C_\beta(THL)\right]dTHL + \int_{-\infty}^{THL} B(THL)\cdot dTHL \end{aligned} \tag{4.10}$$

Global analysis

In a global fit data from all 256 x 256 pixels in a chip are summed and added in a single graph. Since quad detectors have four chips, chip 0,1,2 and 3, the result is four fits per measured target element. Figure 15 shows an example of such a fit.

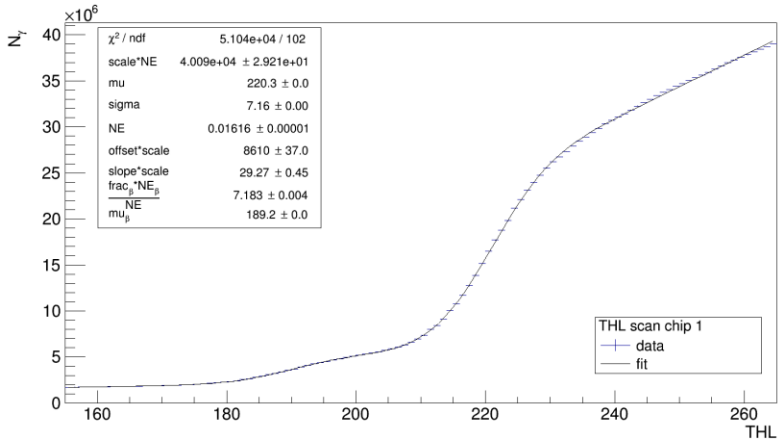

Figure 15: Equation 4.10 fitted through Palladium data measured by chip 0.The vertical axis shows the amount of photons, and the horizontal axis shows THL values. Fitting parameters are shown at the left top. Important parameters are mu and mu_β , which represent the position of Kα and Kβ.

The steepest points in the S-shaped curves correspond to the points of interest, Kα and Kβ. After the S-curve, data continues along a linear path. This linear path is caused by integration of the charge sharing component. Next to the fit on the THL scan, the program also shows the spectrum derived from the fit, as shown in Figure 16.

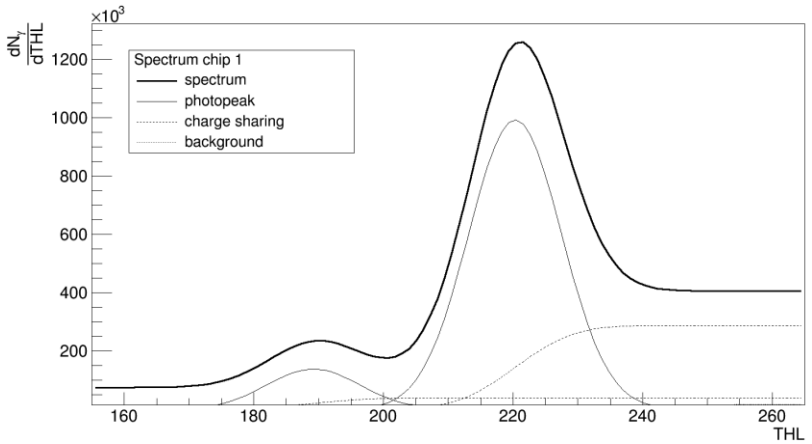

Figure 16: Derivative of the integral spectrum in Figure 15. Various components are individually shown, as well as the sum of all components in the thicker spectrum line.

By comparing the μ values for all target materials with the literature energy values of Kα and Kβ, one could create a calibration for the entire chip. However, a more precise way is to calibrate each pixel individually. The global calibration can then be obtained by averaging the per-pixel parameters.

4.3 Per pixel analysis

Due to the inter pixel mismatches pixel THL values for a given energy are not the same, but are dispersed. By performing a per pixel calibration of the threshold, the pixel energy response can be made as homogeneous as possible. This results in a smaller threshold dispersion between pixels, and improves spectroscopic accuracy of the detector. In order to build a per pixel calibration, all measurements of pure materials of Table 1 need to be fitted on a per pixel basis. The procedure for this is more challenging than the global fit due to the quantity of pixels which need to be fitted. In fact, due to the large amount of parameters in the fitting function 4.10, convergence of the fit strongly depends on the initialization of the

parameters, and fitting boundaries. For this reason a program was developed to fit every pixel automatically. During this project, the program was upgraded to automatically search for initialization values of parameters. The algorithm is organized in steps which gradually increase in complexity. At each stage the estimated parameters are used as initialization values of the next stage. In the following it will be explained how data of a single pixel is fitted. As an example the data from a zirconium measurement is used, shown in Figure 17.

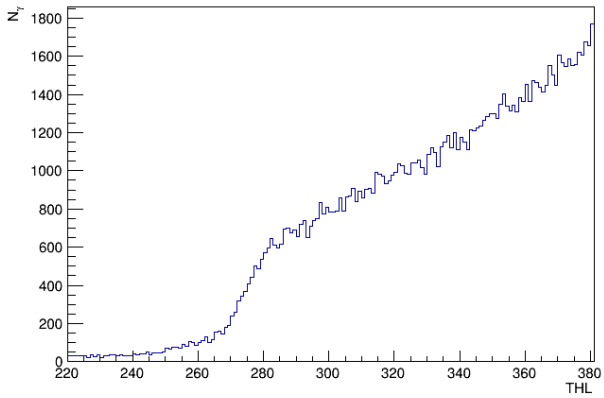

Figure 17: Histogram of a single pixel threshold scan. The measured target is pure zirconium (Zr).

4.3.1 First estimation

Due to the pixel dispersion, it is possible that pixels energy response deviate multiple THL steps from another. The THL range of function 4.10 has to be initialized before the fit and has to be optimized for every single pixel. Therefore a first estimation is made to automatically set an initial Kα value in the fitting function. This initial Kα value is also used to set the minimum and maximum of the THL range.

The initial Kα value is found by taking the derivative of the data and looking for the THL position where the photopeak is most likely to be. However, directly taking the derivative from Figure 17 would lead to high noise in the data. To reduce the noise in the derivative, the THL scan is first smoothened, as shown in Figure 18. Smoothening is performed by averaging photon counts at each THL value with its first neighbors. Figure 19 shows the derivative of the smoothened data.

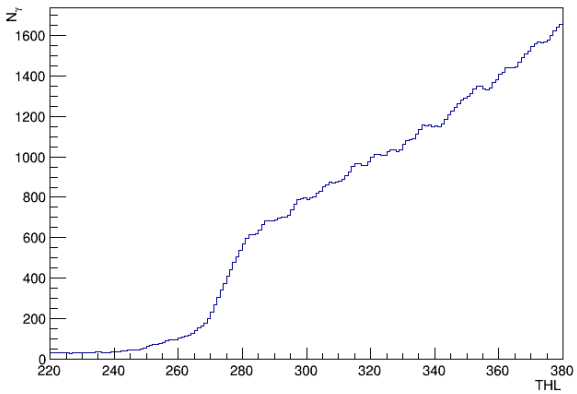

Figure 18: Smoothened data.

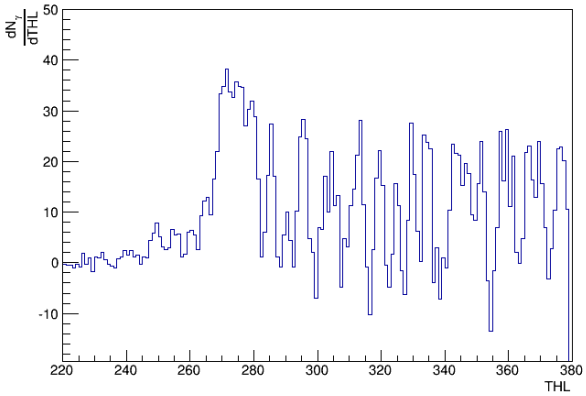

Figure 19: Derivative of the smoothened data.

As can be seen in Figure 19, the smoothened data is still noisy. The histogram is therefore rebinned in 10 intervals, as shown in Figure 20. The rebinned histogram clearly shows the bin containing the Kα peak.

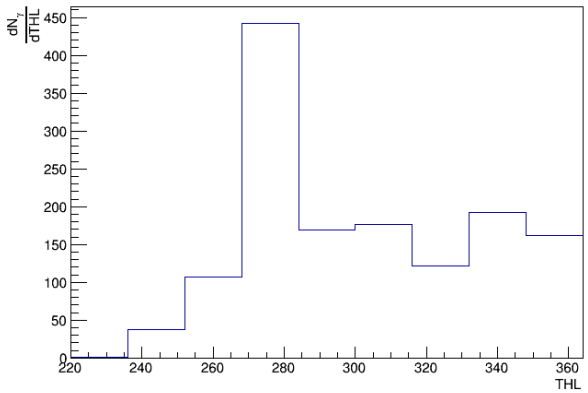

Figure 20: Derivative of the smoothened data, shown in ten intervals.

The central THL value of the highest bin is set as an initialization value of $\mu_{K\alpha}$ This value gives a rough estimation of the Kα location. It is also used to set the minimum and maximum range. The maximum of the THL range is set to be 40 THL above the initialization value of $\mu_{K\alpha}$. The minimum of the range is set to be 30 THL below the initialization value of $\mu_{K\alpha}$ plus an additional THL distance to include the $\mu_{K\beta}$. The additional THL distance is target dependent.

4.3.2 Per pixel fit

First the program fits equation 4.9 (single Gaussian with charge sharing and offset) in Figure 21, using the initial Kα value found in the first estimation. The first fit is used to estimate values for the *scale*, *NE*, Kα and σ.

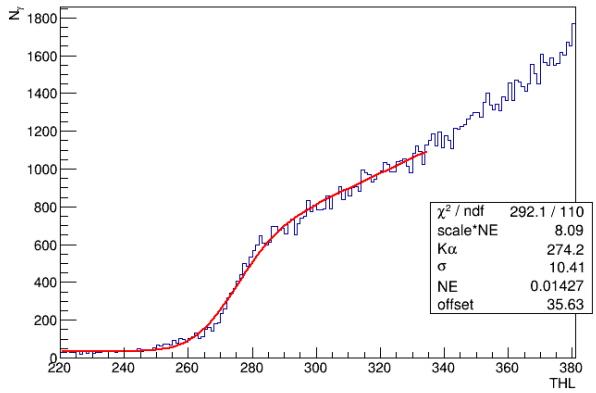

Figure 21: First fit, using equation 4.9.

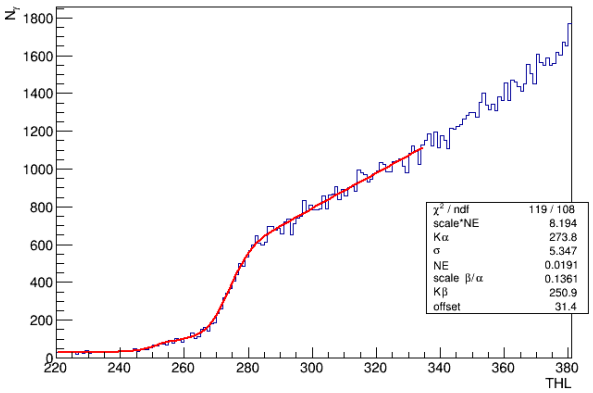

Figure 22: Second fit, using equation 4.10.

After the first fit, a second fit is made, initialized with the estimated parameters of the first fit. The second fit uses equation 4.10, thus containing both Kα and Kβ. Results of the second fit can be seen in Figure 22. Notice the improvement in fit quality (also indicated by χ^2/ndf being close to 1), as well as the reduction in the value of σ. Due to the low statistics at the Kβ position, the initialization of μ_β plays a key role. The initialization value of Kβ is set as a THL position at a fixed distance from Kα. This distance is material dependent, and is determined using the known energy difference between Kα and Kβ and a preliminary rough calibration of THL.

All pixels are fitted for each of the materials in Table 1. Appendix B shows the final result of these measurements for a single pixel.

4.4 Calibration

A calibration allows to determine the relation between energy and THL. Such a calibration is made by plotting the Kα values as measured from the fit, versus the corresponding energy value taken from literature. The values used for the calibration are shown in Table 2, and origin from the fits in Figure 22 and appendix B. Table 2 also contains σ values, which are used to define the uncertainty in THL.

Table 2: Kα calibration values of energy and THL, with σ being the uncertainty of THL. These values are obtained from single pixel fits (Appendix B).

Material	*E* (keV)	Kα (THL) ± σ
Ni	7.477	364.9 ± 6.985
Cu	8.047	358.9 ± 7.091
Zn	8.638	350.0 ± 6.870
Zr	15.774	273.8 ± 5.347
Pd	21.175	217.1 ± 6.132
Ag	22.162	207.4 ± 5.859
In	24.207	186.3 ± 5.973
Sn	25.270	174.0 ± 5.481

The detector is calibrated using only the Kα values because of the lower efficiency of the fit at Kβ. This inefficiency is caused by the low Kβ emission from the target, leading to a low signal to noise ratio.

In the energy range used for this project, the energy - THL relation is linear. Therefore the calibration points are fitted with a first degree polynomial with two parameters; slope and offset. In this calibration the σ of the fit, also shown in Table 1, is used as an error bar of THL. Figure 23 shows the linear calibration through the values of Table 2. In this example the calibration points for each of the measured targets are shown on the final graph. In few cases the fitting of the threshold scan of a given element is not performed correctly, and the corresponding point has to be excluded from the calibration. To verify the quality of the THL scan fit, the χ^2/ndf is evaluated. Only when χ^2/ndf < 3, the corresponding point is used for the calibration.

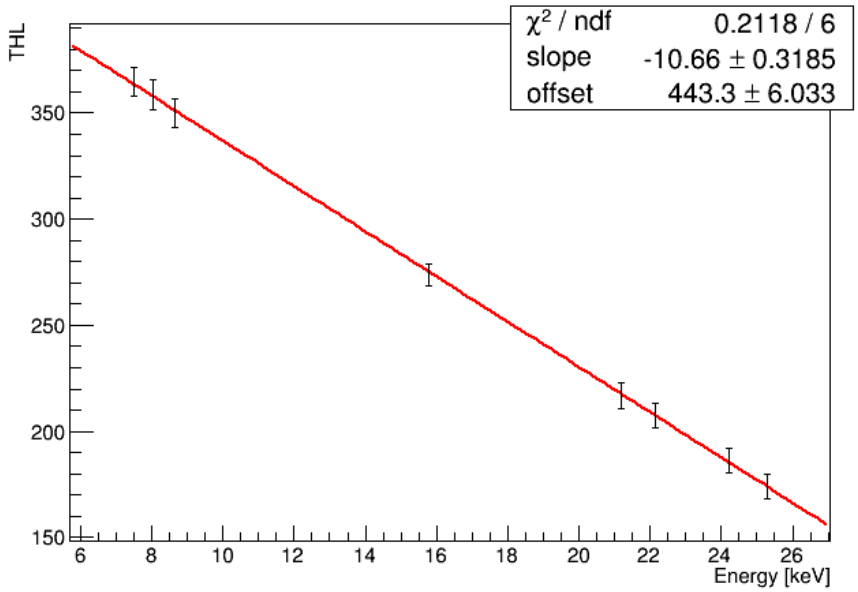

Figure 23: A single pixel calibration.

The calibration line will be used to translate THL values into units of energy. The per-pixel calibration can be used to align the energy response of the whole detector, and therefore optimize its homogeneity and energy resolution.

The process as described in this chapter is repeated for every pixel. Leading to 512 x 512 values of slope and offset. A pixel distribution of the slopes can be seen in Appendix C, as well for the offset in Appendix D.

5 Discussion

A per pixel energy calibration is performed for the quad chip detector Timepix. During the process all measurements are fitted using the algorithm described in chapter 4.2. In the first version of the analysis software, the algorithm was fitting the per pixel scan using directly equation 4.9 and 4.10. These equations were initialized using the results from a global fit, and no per-pixel initialization was implemented. The fit was highly inefficient, less than 75% of the pixels fits converged. Failure to converge repeatedly occurred at the same pixels, for different materials, leading to incorrect calibrations. During this project, the algorithm was improved by adding the multiple stages mechanism. In the current status of the analysis, there is no more need to initialize the parameter values from the global fit, and convergence of the pixels has increased to more than 90%. The enhanced algorithm results in a correct calibration for almost 100% of the pixels. Some examples of fluorescence data fitted with the new algorithm are shown in Appendix B.

The calibration process resulted in 512 x 512 calibration lines, with each values of slope and offset. A distribution of these values per chip can be seen in Appendix C and D. All chips show similar distributions compared to one another. The slope values between chips are similar, approximately just below 11 keV^{-1}. The offset values show differences, with an offset difference of 70 THL between mean values of chips 0 and 3 (Appendix D, Figures 44 and 45).

Appendix C and D also show the advantage of a per pixel calibration instead of a chip calibration. In a chip calibration the average values of slope and offset are determined, and no information about the dispersion can be obtained. With a per pixel calibration it is possible to equalize the pixels in terms of energy, resulting in a smaller dispersion.

6 References

6.1 Publications

[1] Xavier Liopart Cudié, *Design and characterization of 64K pixels chips working in single photon processing mode*. PhD thesis, Mid Sweden University Doctoral Thesis 27, 2007.

[2] Enrico Jr. Schioppa, *Notes*. Draft PhD thesis, NIKHEF, 2013.

6.2 Books

[3] S. O. Kasap, *Optoelectronics And Photonics: Principles And Practice, First Edition.* Published by Prentice Hall, Publication date: 2001 , ISBN: 9780201610871.

[4] Dr. ir. M.T.C. de Loos-Vollebregt, *Spectrometische analysetechnieken*. Published by Syntax Media, 2009, ISBN: 9789077423714.

[5] J. T. Bushberg, J. A. Seibert, E.M. Leidholdt Jr, J. M. Boone, *The essential physics of medical imaging.* Published by Williams & Wilkins, 1994, ISBN: 0-683-01140-5.

[6] H. Spieler, *Semiconductor detector systems*. Published by Oxford University Press Inc., 2005, ISBN: 978-0-19-852784-8

6.3 Web sources

[7] X-ray image: http://www.biomedsearch.com/attachments/00/20/17/75/20177565/JMP-35-3-g002.jpg

[8] Medipix image: http://www.amolf.nl/medipix/medipix-family/

[9] Medipix collaboration site: http://medipix.web.cern.ch/medipix/pages/medipix2/documentation.php

[10] X-ray tube image: httpchemwiki.ucdavis.edu@apidekifiles878=xraytube.png

[11] Bremsstrahlung model: http://www4.nau.edu/microanalysis/Microprobe-SEM/Images/Bremsstrahlung.jpg

[12] Continues spectrum: http://miac.unibas.ch/PMI/01-BasicsOfXray-media/figs/Bremsstrahlung_Spectrum.png

[13] Atom shells: http://www.colorado.edu/physics/phys2170/phys2170_spring96/notes/notes_96.2final90.gif

[14] Superimposed bremsstrahlung and characteristic X-rays: http://upload.wikimedia.org/wikipedia/commons/thumb/3/35/XrtSpectrum.jpg/320px-XrtSpectrum.jpg

A. Appendix: Fit function

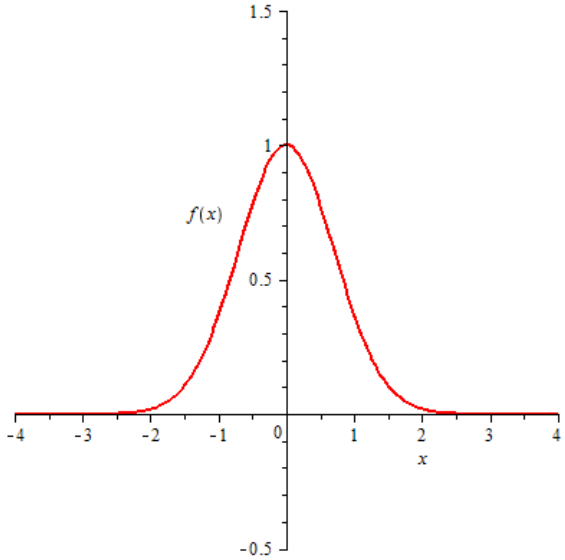

Figure 24: Gaussian function, made with equation 4.4.

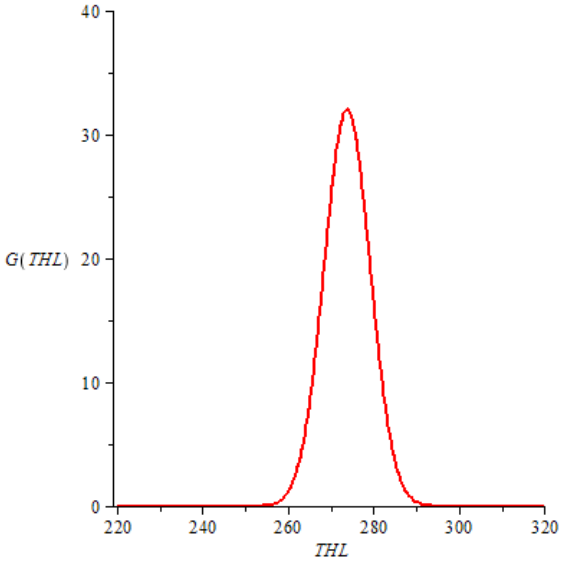

Figure 25: Gaussian made with equation 4.5 ,using: μ=273.8, σ=5.347 and scale= 32.01 (parameters of Figure 22).

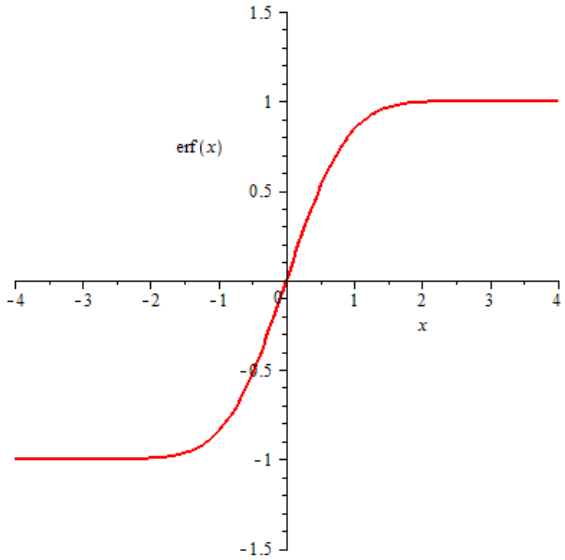

Figure 26: Error function, showing equation 4.6.

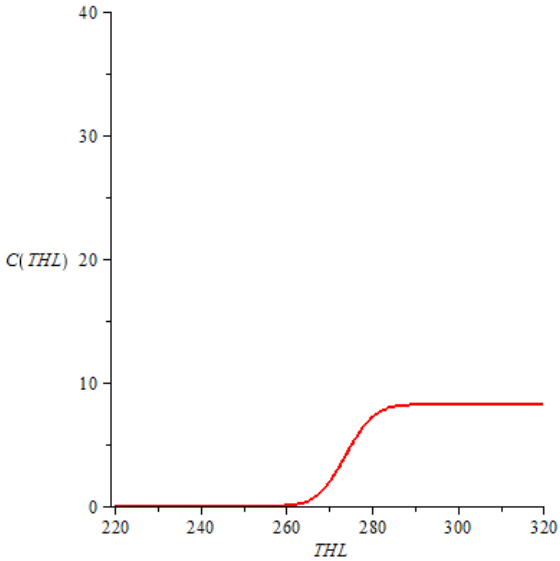

Figure 27: Error function, made with equation 4.7, using: μ=273.8, σ=5.347 and scale·NE= 8.194 (parameters of Figure 22).

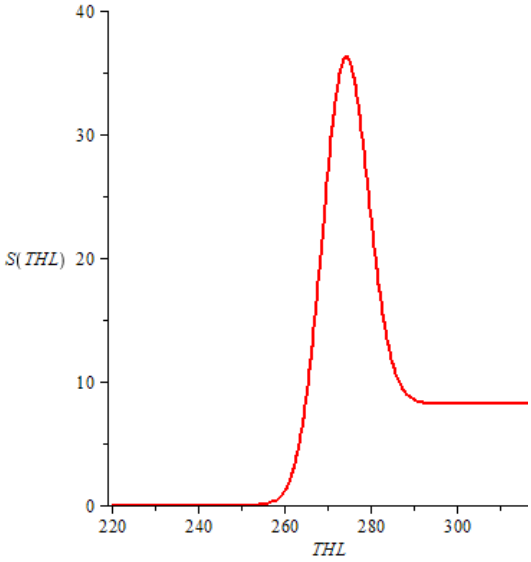

Figure 28: Gaussian plus charge sharing made with equation 4.8 ,using: μ=273.8, σ=5.347 and scale·NE= 8.194 (parameters of Figure 19).

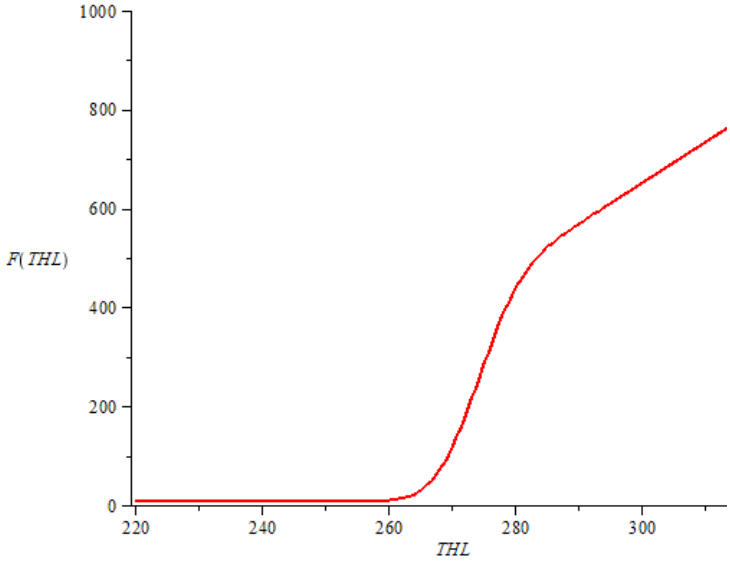

Figure 29: Integral of figure 28, also described in equation 4.9

B. Fits of different materials

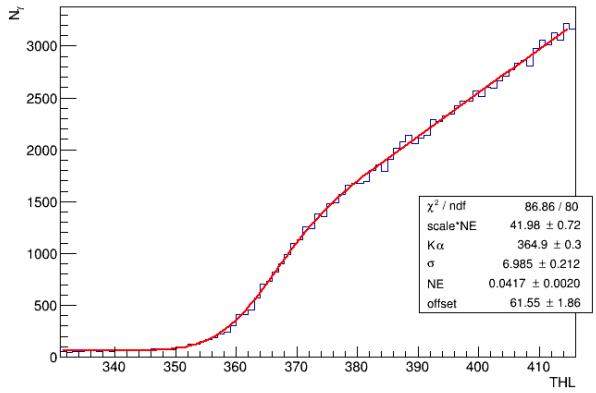

Figure 30: Ni measurement, Kβ is close to Kα and cannot be distinguished

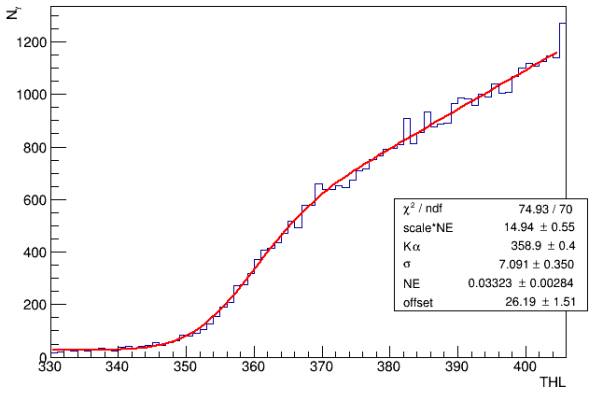

Figure 31: Cu measurement, Kβ is close to Kα and cannot be distinguished

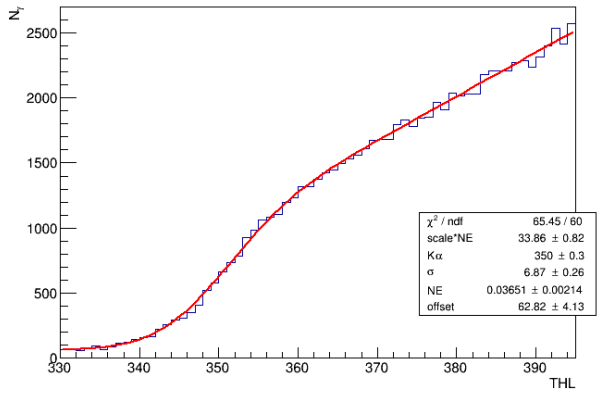

Figure 32: Zn measurement, Kβ is close to Kα and cannot be distinguished.

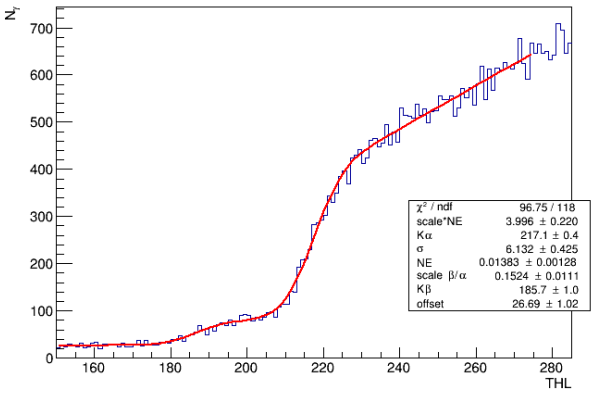

Figure 33: Pd measurement.

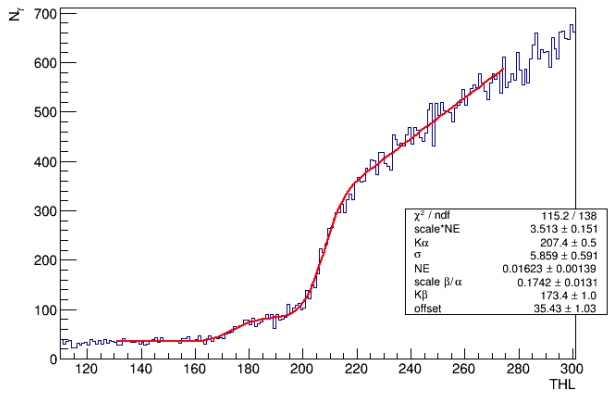

Figure 34: Ag measurement.

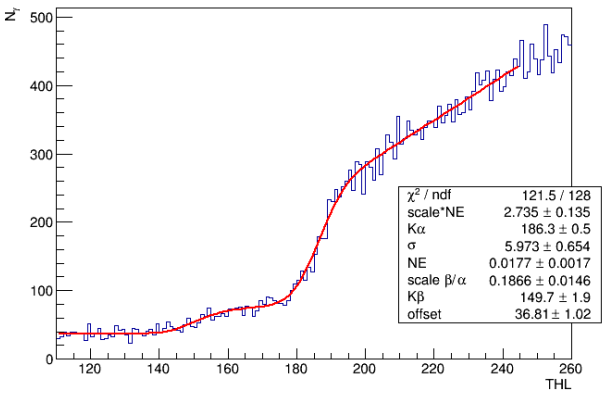

Figure 35: In measurement.

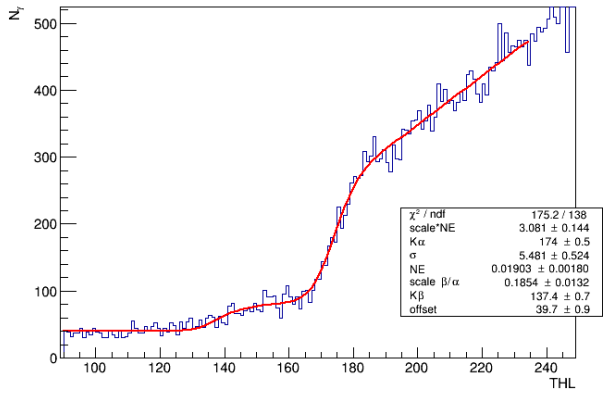

Figure 36: Sn measurement.

C. Slope distribution

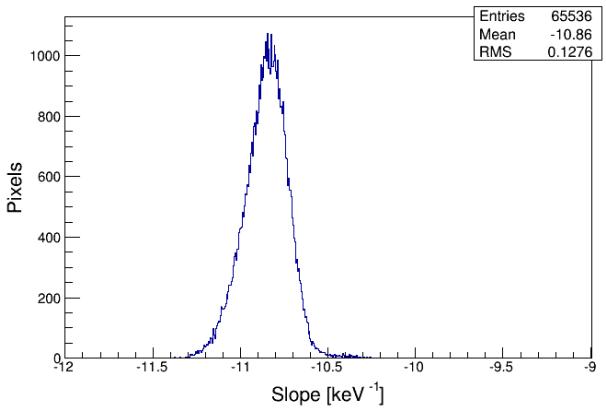

Figure 37: Distribution of pixels per slope value in chip1.

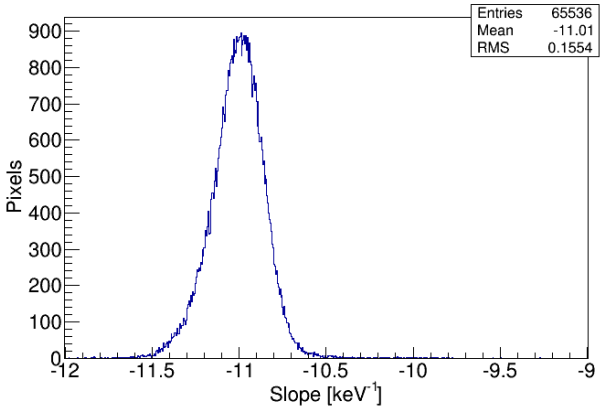

Figure 38: Distribution of pixels per slope value in chip3.

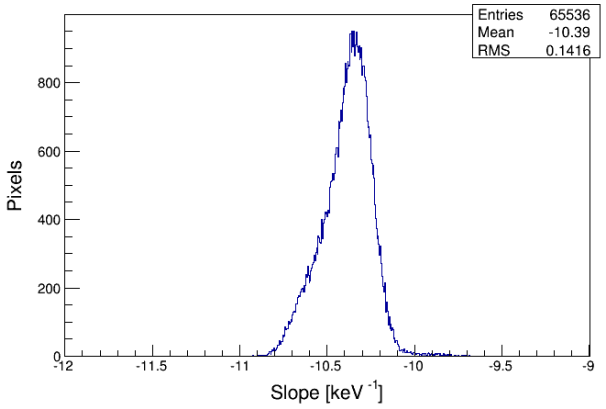

Figure 39: Distribution of pixels per slope value in chip 0.

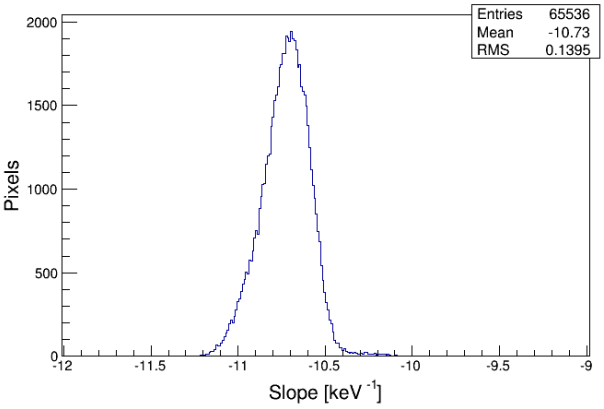

Figure 40: Distribution of pixels per slope value in chip2.

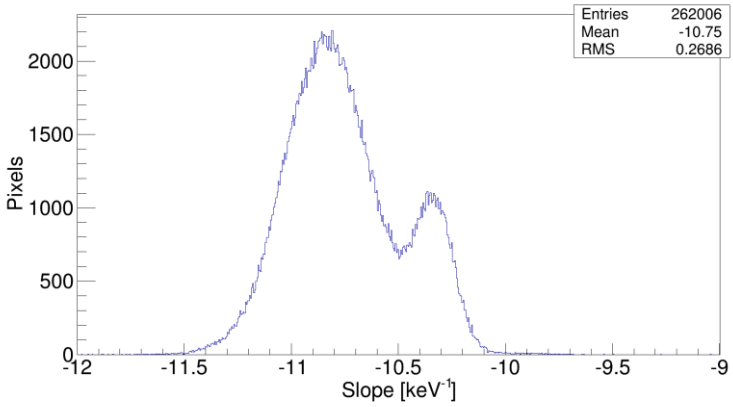

Figure 41: Distribution of pixels per slope value of all four chips.

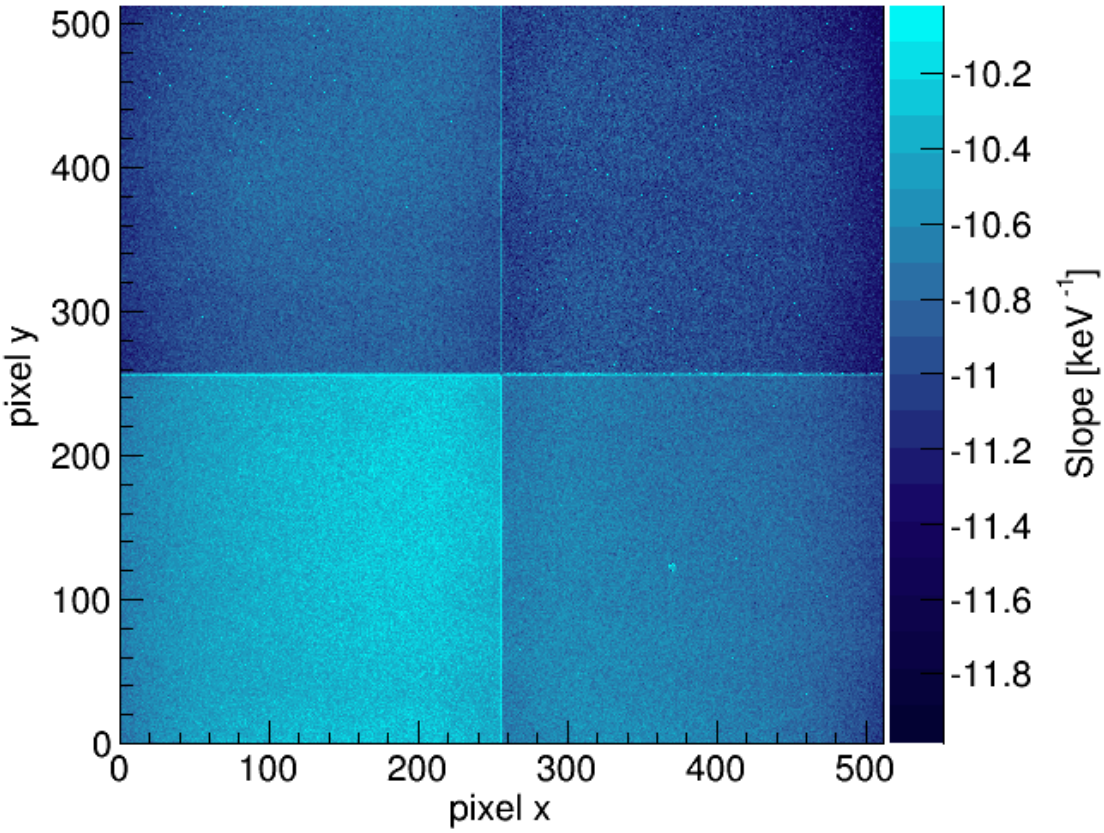

Figure 42: Slope values of each pixel. The chips are ordered in the same way as Figure 37 – 40.

D. Offset distribution

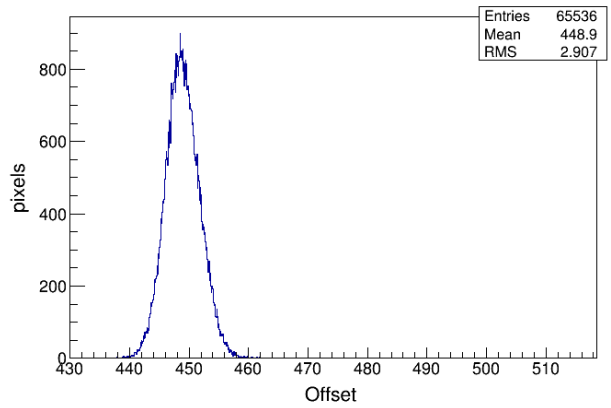

Figure 43: Distribution of pixels per offset in chip 1.

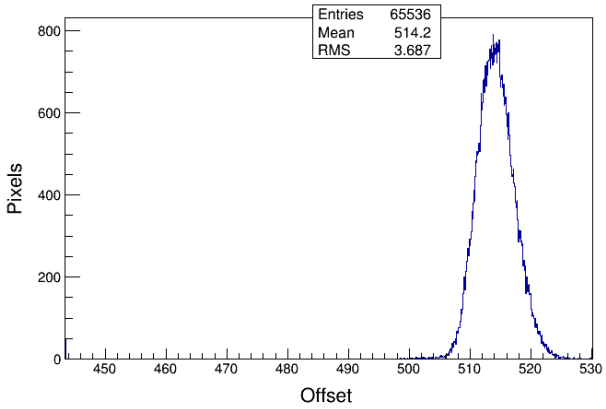

Figure 44: Distribution of pixels per offset in chip 3.

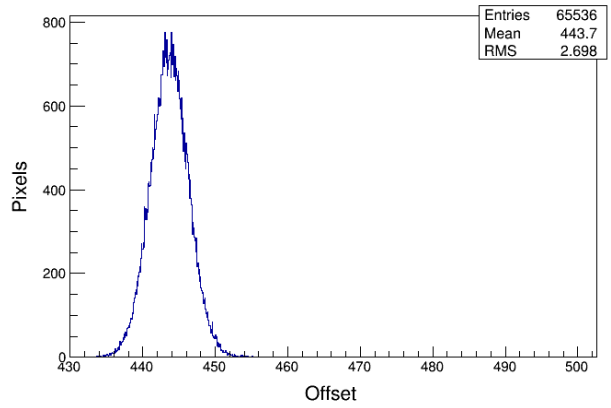

Figure 45: Distribution of pixels per offset in chip 0.

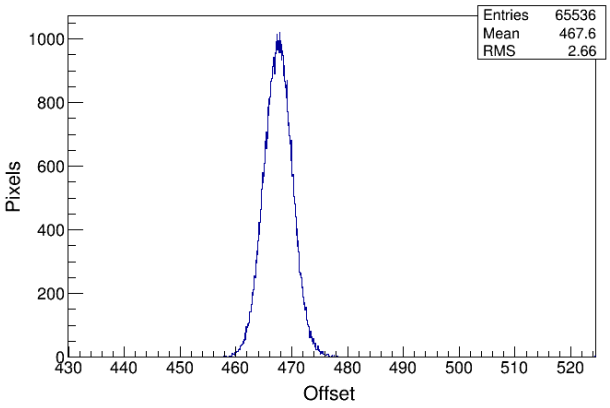

Figure 46: Distribution of pixels per offset in chip 2.

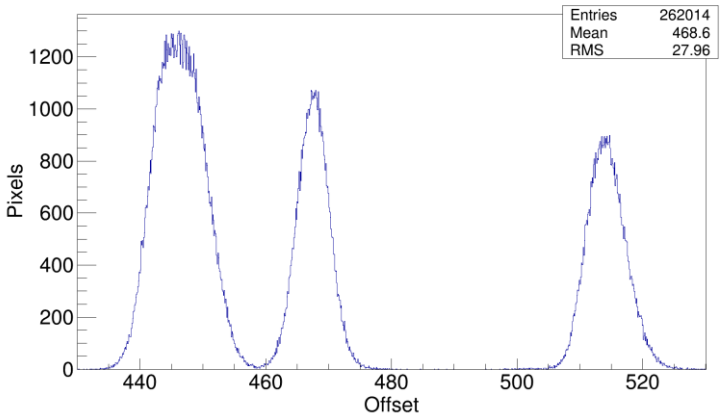

Figure 47: Distribution of pixels per offset, showing all chips in the quad detector

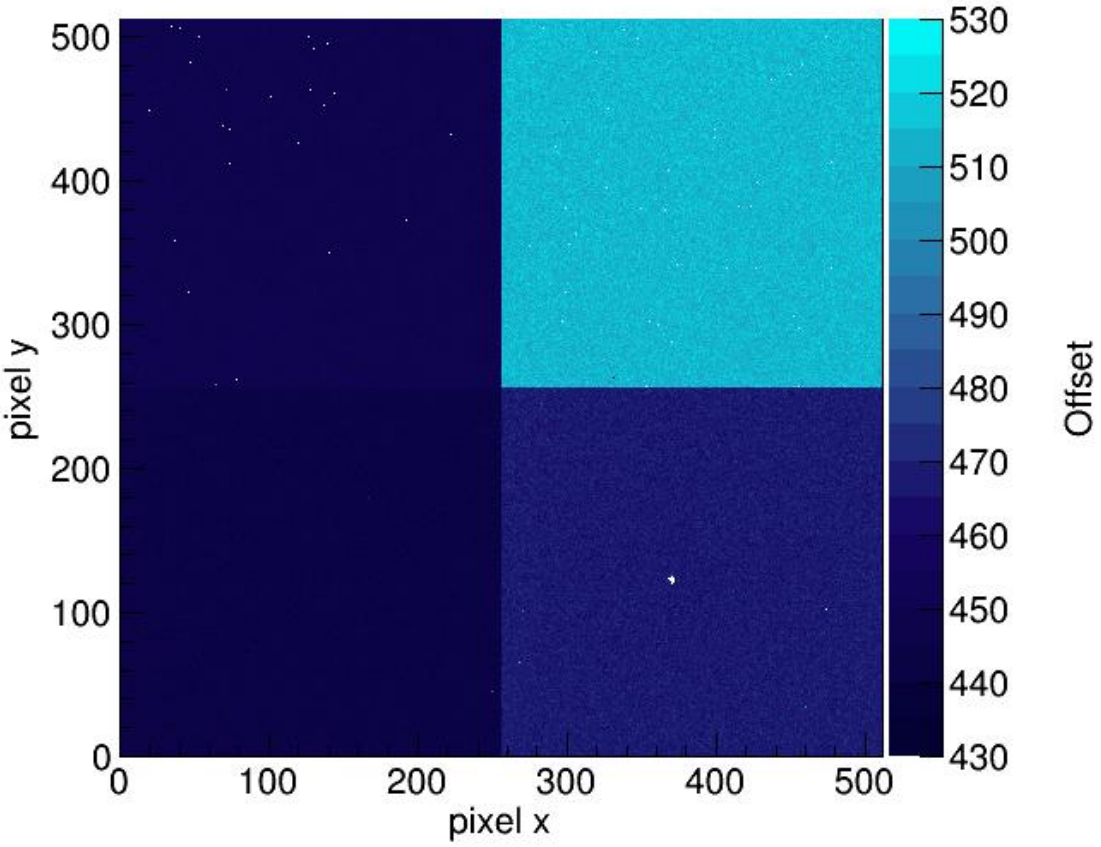

Figure 48: Offset values of each pixel. The chips are placed in the same order as in Figure 43 – 46.

E. Hamamatsu X-ray tube documentation

X-RAY SOURCE

90 kV MICROFOCUS X-RAY SOURCE L9421-02

FEATURES

● Focal Spot Size: 5 μm (at 4 W)
The focal spot of 5 μm of the sealed type X-ray tube enables sharp and clear X-ray images even at a high magnification.

●Easy Handling
Fully operable from an external PC.

●Serial Port Control (RS-232C)
One package of a sealed type X-ray tube, a high-voltage power supply and a control function.

APPLICATIONS

●Non-destructive Inspection
●X-ray CT
●In-line X-ray Inspection

[Applicable Objects]
- **Electronic component**
- **Printed circuit board**
- **Plastic component**
- **Metal component**

HAMAMATSU

SPECIFICATIONS

GENERAL

Parameter	Description / Value	Unit
Input Voltage (DC)	+24	V
Power Consumption (Max.)	96	W
X-ray Leakage ① (Max.)	1	mSv/h
Operating Ambient Temperature	+10 to +40	°C
Storage Temperature	0 to +50	°C
Operating and Storage Humidity	Below 85 (No Condensation)	%
Weight	Approx. 10	kg
Conformance Standards	CE (IEC61326)	—
Operation	Continuous	—
High Voltage Power Supply	Built-in	—

X-RAY TUBE

Parameter	Description / Value	Unit
X-ray Tube	Sealed Type	—
X-ray Tube Cooling Method	Convection Cooling	—
X-ray Tube Window Material / Thickness	Beryllium / 150	μm
Target Material	Tungsten	—
Tube Voltage Operational Range	20 to 90	kV
Tube Current Operational Range ②	10 to 200 (8 W Max.)	μA
Maximum Output	8	W
X-ray Focal Spot Size	7 (5 μm at 4 W)	μm
X-ray Beam Angle (Coned)	39	degrees
Focus to Object Distance (FOD)	9.5	mm

X-RAY CONTROL PART

Parameter	Description	Unit
Function	Tube Voltage and Tube Current Preset / Auto Warm-up	—
Protection	Interlock	—
External Control	RS-232C	—
Applicable OS	Windows® 2000 Professional, XP Professional	—
Computer Operating Conditions	CPU: Intel Pentium or Higher, Memory: 64 MB or More	—

NOTE: ①Measurement at 1 m from the X-ray focal spot.
②See the graph of the tube current operational range.

⚠ PRE-CAUTION TO USE

1. X-ray emitted from this device is harmful for human body. And it should be necessary for the operator to protect himself/herself from it.
2. During an operation, the X-ray tube unit should be installed in the X-ray shielded facility or area in order to avoid any X-ray leakage. Also the interlock system in X-ray control unit should be always used in order to avoid any misoperation.

OPERATIONAL CAUTION

The product may be subject to governmental occupational radiation hazardous regulation therefore the necessary application must be field according to the local regulation.

TUBE CURRENT OPERATIONAL RANGE

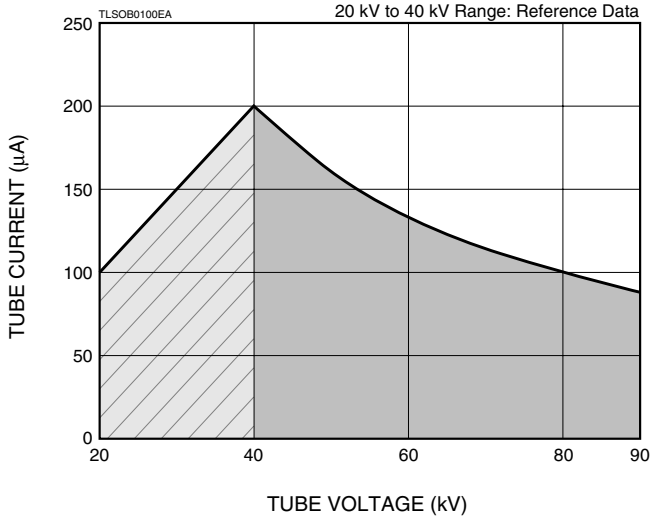

DIMENSIONAL OUTLINE (Unit: mm)

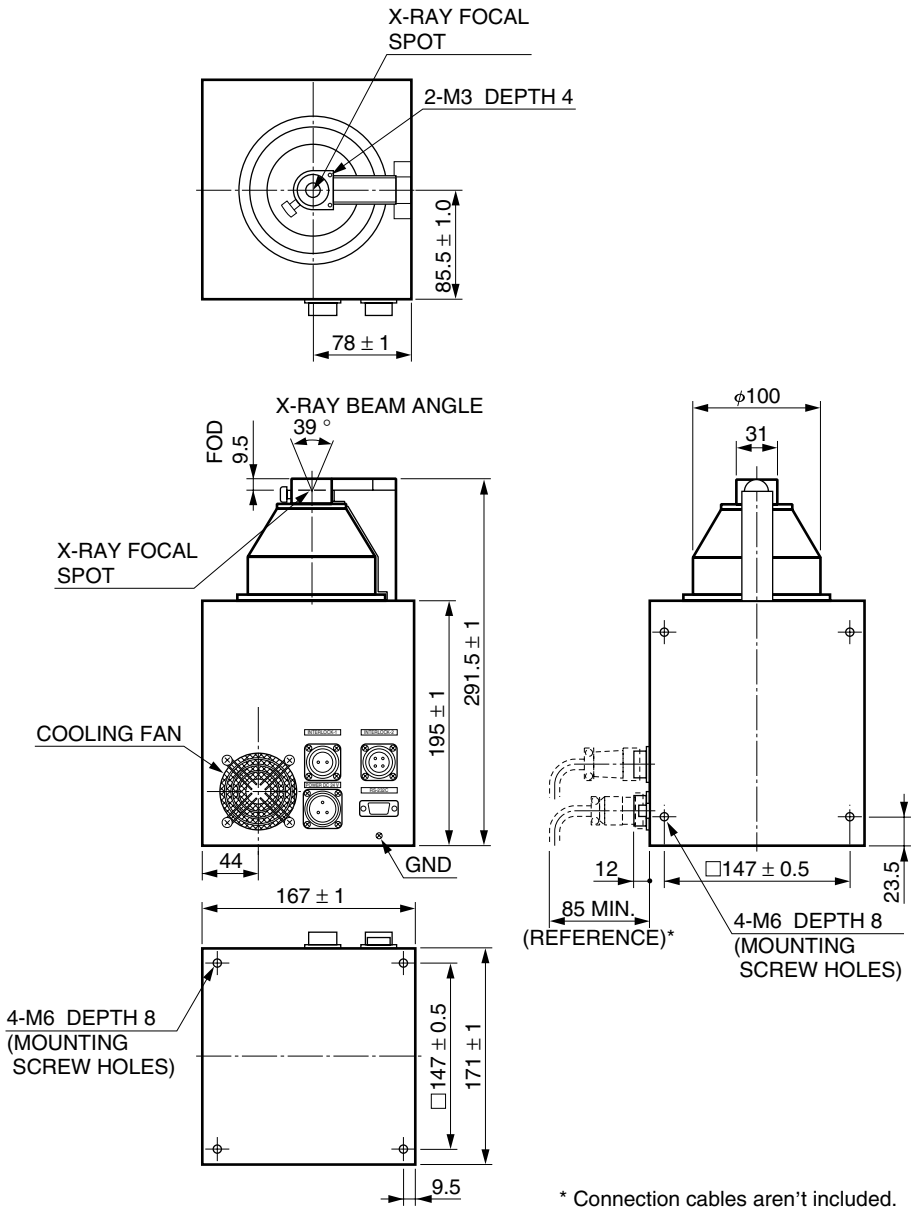

* Connection cables aren't included.

TLSOA0093ED

F. Project proposal

Spectroscopic X-ray imaging with detectors of the Medipix family

Project proposal
Nikhef detector R&D group
Enrico Jr. Schioppa
10-01-2012

Introduction

Pixel devices are used in modern detectors at particle accelerator experiments. Since few years the possibility to apply these systems to other fields has been of great interest.
Pixel detectors are composed of a sensor and a readout. The sensor is the layer where a particle is actually detected: here the energy transferred to the medium is converted into charge carriers. These are then drifted to the readout where they give rise to an electric signal.
The detectors of the Medipix family are pixel detectors in which a first processing of the signal takes place directly inside the single pixel. The most important feature is the possibility to estimate the amount of charge produced by the particle, which is proportional to the energy which was released. The detector thus acquires spectroscopic (i.e. energy resolving) capabilities.
When these detectors are used in the field of X-ray imaging, the possibility to add energy estimation to single X-ray photons opens a wide range of improvements with respect to conventional systems.

Project proposal A: effect of per-pixel calibration on energy resolution

Although all pixels are designed to be exact copies of each other, it is impossible that they are all manufactured the same way. Mismatches are unavoidable.
In order to ensure the best performance from a spectroscopic detector, it is important that the energy response of the pixels is as more homogeneous as possible. A pixel equalization procedure is therefore crucial.
A first pixel matrix equalization procedure is already available in the software package used to operate Medipix chips. However, this is not enough. To maximize the homogeneity of the matrix response, a per-pixel energy calibration is necessary.
Such a calibration can be performed by exploiting the (almost) monochromatic radiation emitted as fluorescences from pure metal samples excited by a primary X-ray field.
In the project the student will get familiar with this technique and will study how an energy calibration driven equalization of the pixel matrix is able to optimize the performance of the detector.

Project proposal B: operation of the CT setup

X-ray computerized tomography (X-CT) is the technique that allows to reconstruct the 3D structure of the inner part of a body imaged with X-rays. The principle of CT reconstruction is relatively simple: if an object is (X-ray) imaged from different points of view, a proper mathematical treatment of the collection of 2D images allows to estimate the 3D structure of the original object.

At Nikhef an X-ray CT setup for micro-imaging with Medipix based detectors has been recently built in order to study how these techniques can benefit from the spectroscopic capabilities of such devices.

In this project the student will get familiar with the operation of the CT setup and the detector data acquisition system for X-ray images, contributing to the collection of CT data for further analysis.